Preparation behavior in a Hanks' solution on Ca-P-O films prepared by laser CVD

Materials Transactions, Vol. 50, No. 10 (2009) pp. 2455 to 2459

Precipitation Behavior in a Hanks' Solution on Ca-P-O Films Prepared by Laser CVD

Mitsutaka Sato[1], Rong Tu[2], Takashi Goto[2], Kyosuke Ueda[3] and Takayuki Narushima[3]

[1]*Osaka Center for Industrial Materials Research, Tohoku University, Sakai 599-8531, Japan*
[2]*Institute for Materials Research, Tohoku University, Sendai 980-8577, Japan*
[3]*Department of Materials Processing, Tohoku University, Sendai 980-8579, Japan*

Ca-P-O films were prepared by laser CVD using $Ca(dpm)_2$ and $(C_6H_5O)_3PO$ metal organic precursors. The crystal phase of Ca-P-O films changed depending on deposition temperature (T_{dep}), total pressure (P_{tot}), laser power (P_L) and molar ratio of Ca to P ($R_{Ca/P}$). β-TCP films in a single phase were obtained in a P-rich and high T_{dep} region, while HAp films in a single phase were obtained in a Ca-rich and low T_{dep} region. The β-TCP films had a (220) orientation with an elongated and angular roof-shaped surface texture, whereas HAp films had a (300) orientation with a granular surface texture. Both the β-TCP film and the HAp film had a dense cross section. The Ca-P-O films were immersed in a Hanks' solution for 6 h to 7 d. Particle-shaped precipitates were observed on the β-TCP and HAp films after 3 d immersion. Needle-shaped precipitates covered the whole surface of HAp film after 7 d immersion. [doi:10.2320/matertrans.M2009160]

(Received May 7, 2009; Accepted July 7, 2009; Published August 19, 2009)

Keywords: *laser chemical vapor deposition (CVD), β-tricalcium phosphate, hydroxyapatite, Hanks' solution*

1. Introduction

Ti and its alloys have been widely used in artificial implants such as artificial hip joints and teeth implants because of their good mechanical properties, corrosion resistance and biocompatibility.[1,2] However, it takes more than 3 months for Ti alloys to adhere to bones.[3,4] In order to shorten the adherence time, bio-ceramic films on implants have been widely investigated by using sol-gel,[5,6] plasma spray,[7,8] sputtering[9,10] and an alkali heating process.[11,12]

Chemical vapor deposition (CVD) is advantageous to obtain a wide range of films at a relatively high deposition rate with good morphology controllability and good adherence to substrates, as commonly demonstrated in the preparation of TiO_2[13] and ZrO_2[14] films. In our previous work, we prepared calcium titanate ($CaTiO_3$),[15] α-tricalcium phosphate (α-$Ca_3(PO_4)_2$, α-TCP) and hydroxyapatite ($Ca_{10}(PO_4)_6(OH)_2$, HAp)[16] films by MOCVD and immersed them in a pseudo body fluid to investigate apatite regeneration behavior.[17,18] In the case of $CaTiO_3$ films, the apatite regeneration rate significantly depended on the surface morphology of films, and the nucleation of apatite occurred at hollow places on the film surface. However, in the case of α-TCP and HAp films prepared by MOCVD, a smooth and dense microstructure was obtained. If Ca-P-O films had a more complicated surface morphology, the precipitation would be more promoted.

We have previously reported the use of the laser chemical vapor deposition (LCVD) process to prepare Ca-P-O films on alumina substrates.[19] α-TCP and HAp films in a single phase were obtained and their surface morphology had a more complicated texture compared with those prepared by MOCVD, where α-TCP film had orientations of (290) and (400), while HAp film showed orientations of (002) and (300) when the deposition conditions were changed.

In the present study, Ca-P-O films were prepared on CP-Ti substrates by LCVD, and the precipitate regeneration behavior on the Ca-P-O films prepared on CP-Ti substrates by LCVD was studied in a Hanks' solution.

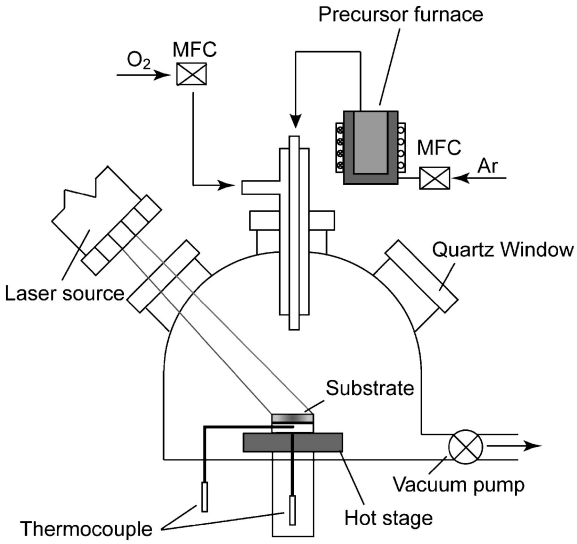

Fig. 1 Schematic of laser CVD apparatus.

2. Experimental Procedures

Ca-P-O films were prepared by a vertical cold-wall type LCVD apparatus. Figure 1 is a schematic of the LCVD apparatus. $Ca(dpm)_2$ (bis-dipivaloylmethanato-calcium) and $(C_6H_5O)_3PO$ (triphenylphosphate) precursor powders were evaporated at 523 to 573 and 493 to 533 K, respectively. The molar ratio of Ca to P ($R_{Ca/P}$) was controlled by changing the evaporation temperature (T_{eva}). The precursor vapors were carried into the reactor by Ar gas. O_2 gas was separately introduced by a double-tube nozzle. The total gas flow rate ($FR_{tot} = FR_{Ar} + FR_{O_2}$) was fixed at 3.33×10^{-6} m^3 s^{-1}. The substrate was pre-heated (T_{pre}) at 673 to 873 K. The total pressure (P_{tot}) in the CVD reactor was kept at 0.6 kPa. A Nd:YAG laser (wavelength, $\lambda = 1064$ nm) was irradiated to a substrate through a quartz window. The size of the laser beam was expanded by an optic lens to about 15 mm in diameter. The laser power (P_L) was changed from 0

Table 1 Deposition conditions of Ca-P-O films.

Precursor	$Ca(dpm)_2$
	$(C_6H_5O)_3PO$
Vaporization temperature (T_{prec})	553–593 K ($Ca(dpm)_2$)
	473–513 K ($(C_6H_5O)_3PO$)
Substrate	CP-Ti
Laser power (P_L)	30–50 W
Preheating temperature (T_{pre})	673–873 K
Total pressure (P_{tot})	0.6 kPa
Ar gas flow rate (F_{Ar})	8.3×10^{-7} m^3s^{-1} (50 sccm)
O_2 gas flow rate (F_{O_2})	1.6×10^{-6} m^3s^{-1} (100 sccm)
Distance between nozzle and substrate (d)	20 mm
Deposition time	10 min

Table 2 Chemical composition of Hanks' solution.

Concentration (g/m^3)							
NaCl	KCl	Na_2HPO_4	KH_2PO_4	$MgSO_4$	$MgCl_2$	$CaCl_2$	Glucose
8000	400	47.9	60	48.8	46.8	140	1000

to 200 W. A commercially pure titanium (CP-Ti) plate ($10 \times 10 \times 1.0$ mm) was used as a substrate. A thermocouple was inserted into a pre-cut slot at the backside to measure deposition temperature (T_{dep}). The distance between the nozzle and the substrate was fixed at 20 mm. The deposition conditions are summarized in detail in Table 1. The crystal structure of the films was analyzed by X-ray diffraction (XRD). The microstructure and thickness were examined by scanning electron microscopy (SEM). Precipitation behavior on Ca-P-O film was investigated by an immersion test in a Hanks' solution for 6 h to 7 d. The composition of the Hanks' solution is listed in Table 2.

3. Results and Discussion

Figure 2 shows the relationship between P_L and T_{dep} for Al_2O_3 and CP-Ti substrates. The T_{dep} increased with increasing P_L and the T_{dep} of CP-Ti substrate was slightly higher than that of the Al_2O_3 substrate. This may have been caused by the laser absorbance of CP-Ti being higher than that of Al_2O_3.[20,21] Since the surface of the CP-Ti substrate was partially melted at $P_L > 50$ W, the deposition of Ca-P-O films on the CP-Ti substrates was conducted at $P_L \leq 50$ W.

Figure 3 shows the relationship between the evaporation rate of precursors (R_{eva}) and the T_{dep} of CP-Ti substrate. The T_{dep} increased with increasing P_L under the same T_{pre}. However, the T_{dep} was almost independent of R_{eva}. We have previously reported that plasma appeared around the substrate due to the interaction between laser emission and exothermic chemical reactions between precursor vapors and O_2 gas. The plasma combined with the laser emission to the substrate caused the temperature increase from T_{pre} to T_{dep}. Since the P_L was small at less than 50 W, the temperature increase ($\Delta T = T_{dep} - T_{pre}$) was 100 to 200 K, almost independent of R_{eva}.

Figure 4 shows a CVD phase diagram of Ca-P-O films prepared on CP-Ti substrate at $P_L = 30$ W and $P_{tot} = 0.6$ kPa. At $T_{dep} > 850$ K and $R_{Ca/P} < 0.45$, mixed phases of HAp and β-TCP were obtained. At $T_{dep} = 750$ to 850 K,

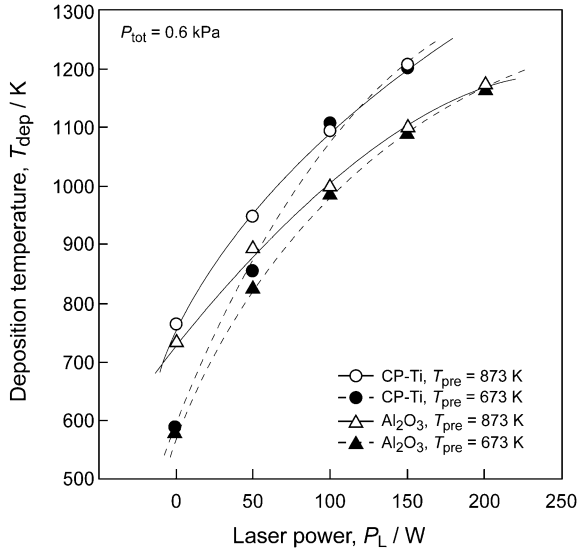

Fig. 2 Relationship between T_{dep} and P_L for alumina and CP-Ti substrate.

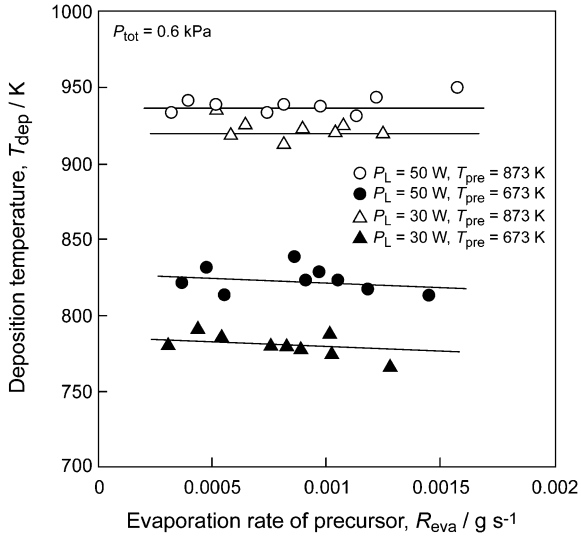

Fig. 3 Relationship between T_{dep} and R_{eva} at $P_{tot} = 0.6$ kPa.

$R_{Ca/P} < 0.45$ and at $T_{dep} > 850$ K, $R_{Ca/P} = 0.45$ to 0.6, HAp films in a single phase were obtained, whereas at $R_{Ca/P} > 0.6$, mixed phases of HAp and tetracalcium phosphate (TTCP, $Ca_4(PO_4)_2O$) or those of HAp and CaO were obtained. A CaO phase tended to be co-deposited in a low T_{dep} region.

Figure 5 shows a CVD phase diagram of Ca-P-O films prepared on a CP-Ti substrate at $P_L = 50$ W and $P_{tot} = 0.6$ kPa. At $T_{dep} > 900$ K and $R_{Ca/P} < 0.4$, β-TCP in a single phase was obtained. At $T_{dep} > 900$ K, $R_{Ca/P} = 0.4$ to 1.0 and at $T_{dep} < 900$ K, $R_{Ca/P} < 0.45$, a mixed phase of β-TCP and HAp was obtained. At $T_{dep} > 900$ K, $R_{Ca/P} > 1.0$ and $T_{dep} < 900$ K, $R_{Ca/P} > 0.45$, HAp in a single phase was obtained. Comparing with Fig. 4, CaO and TTCP were not identified at $P_L = 50$ W. In general, CaO cannot react with P-compounds at a low temperature probably less than $T_{dep} = 800$ K as can be seen from Fig. 4. At $P_L = 50$ W, due to the high P_L, the T_{dep} was always more than 800 K and then no CaO was identified. The reactivity of P-compounds with CaO is rather low. Due to higher excitation in higher P_L, the P richer compounds could be likely to form at higher P_L. This may be

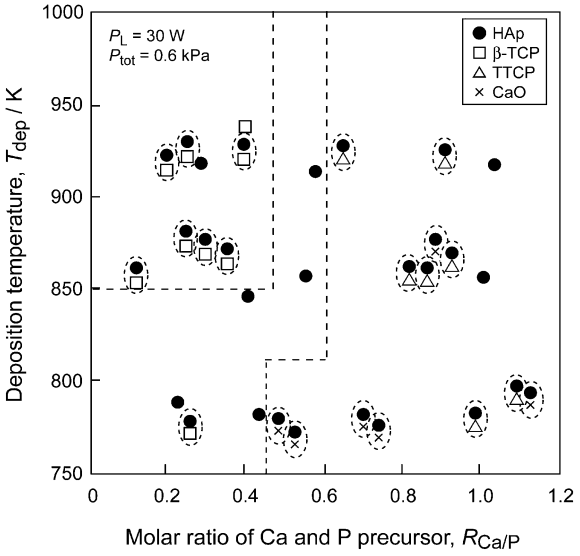

Fig. 4 CVD phase diagram of Ca-P-O films prepared at $P_L = 30$ W and $P_{tot} = 0.6$ kPa.

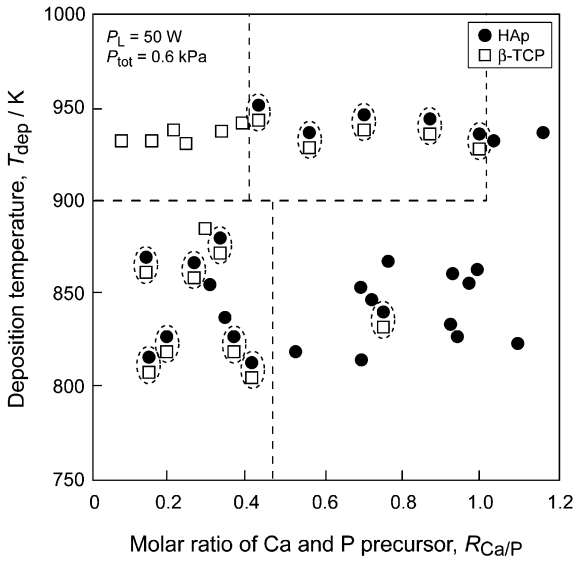

Fig. 5 CVD phase diagram of Ca-P-O films prepared at $P_L = 50$ W and $P_{tot} = 0.6$ kPa.

the reason of the formation of TTCP at $P_L = 50$ W, but not at even the same T_{dep} as shown in Figs. 4 and 5. Generally, in common thermal CVD, the kind of deposited phases are primarily determined thermodynamically by temperature (T_{dep}) and chemical potentials of source gases. On the other hand, the deposited phases in the present LCVD were significantly affected by P_L, suggesting that the laser itself affected the deposited phase due to photochemical effects.

Figure 6 shows XRD patterns of β-TCP and HAp films prepared on CP-Ti substrate at $P_L = 50$ W and $P_{tot} = 0.6$ kPa. The lattice parameters of β-TCP film were $a = 1.042$ and $c = 3.731$ nm, almost in agreement with the literature data of β-TCP (hexagonal, $a = 1.0429$ and $c = 3.738$ nm).[22] The lattice parameters of HAp ($a = 0.946$ and $c = 0.687$ nm) were also close to the values of HAp films prepared by MOCVD.[19] β-TCP and HAp films had significant orientations of (220) and (300), respectively.

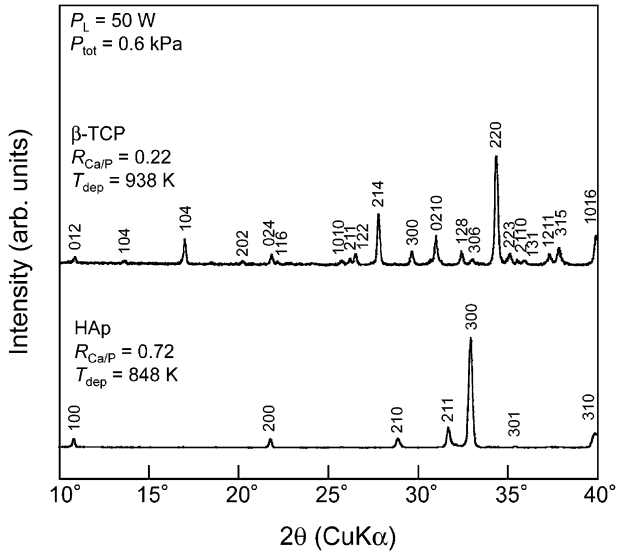

Fig. 6 XRD patterns of β-TCP and HAP films prepared at $R_{Ca/P} = 0.22$ and $T_{dep} = 938$ K (a) and $R_{Ca/P} = 0.72$ and $T_{dep} = 848$ K (b), respectively. ($P_L = 50$ W, $P_{tot} = 0.6$ kPa)

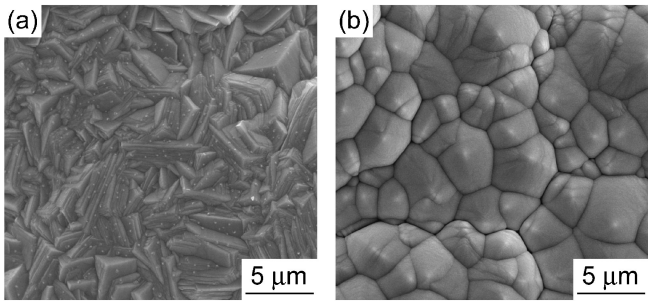

Fig. 7 Surface morphology of β-TCP and HAp films prepared at $R_{Ca/P} = 0.19$ and $T_{dep} = 933$ K (a) and $R_{Ca/P} = 1.16$ and $T_{dep} = 936$ K (b), respectively. ($P_L = 50$ W, $P_{tot} = 0.6$ kPa)

Figure 7 shows the surface morphology of β-TCP and HAp films prepared on CP-Ti substrate at $P_L = 50$ W and $P_{tot} = 0.6$ kPa. The surface morphology of β-TCP film showed an elongated and angular roof-shaped texture that is often observed in (110)-oriented films (Fig. 7(a)). The cross-sectional morphology of β-TCP had a dense texture 10 μm in thickness. The surface morphology of HAp film had a granular texture 3 μm in diameter (Fig. 7(b)), similar to that of HAp film prepared on Al_2O_3 substrate by laser CVD, as previously reported.[19] The cross-sectional morphology of HAp film also had a dense texture.

Figure 8 shows the surface morphology of β-TCP film prepared on CP-Ti substrate at $P_L = 50$ W and $P_{tot} = 0.6$ kPa before and after immersion in a Hanks' solution. Almost no changes were observed until 24 h of immersion (Fig. 8(b), (c)). The edges of the roof-shaped crystals in the β-TCP film became round after 3 d (Fig. 8(d)). It is known that β-TCP may dissolute in a simulated body fluid more than HAp.[23] The microstructure change may be related to the dissolution of β-TCP film. Spherical particles were preferentially precipitated at hollow places on the β-TCP film after 3 d (Fig. 8(d)). In our previous study, similar precipitates were observed on α-TCP films prepared by MOCVD after

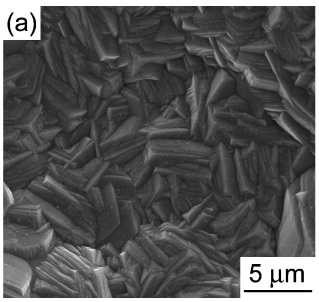

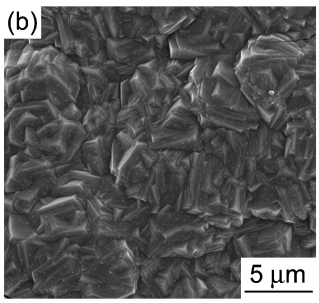

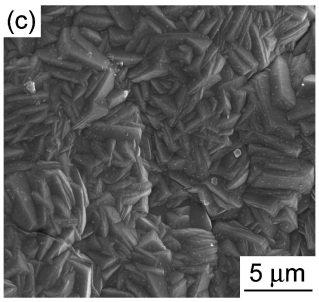

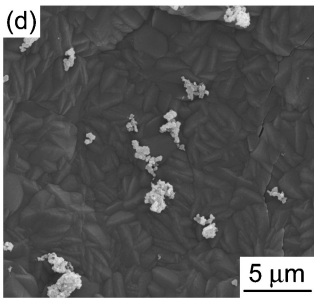

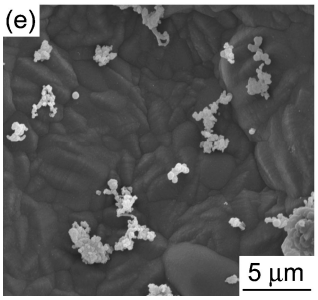

Fig. 8 Surface morphology of β-TCP film (a) before immersion and after immersion in a Hanks' solution for (b) 6 h, (c) 24 h, (d) 3 d and (e) 7 d.

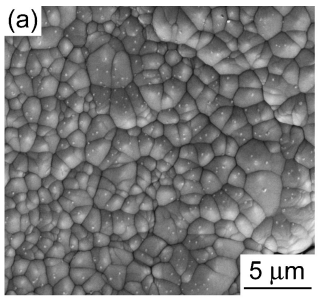

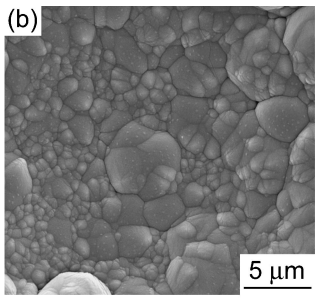

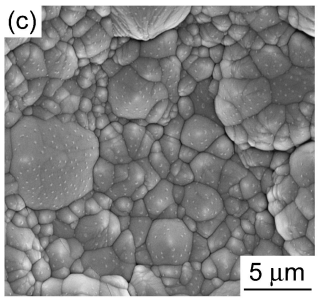

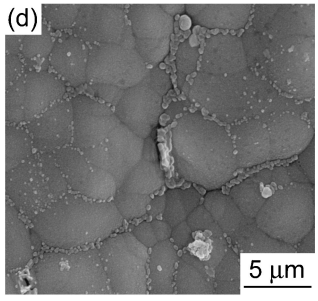

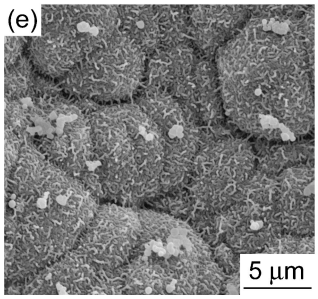

Fig. 9 Surface morphology of HAp film (a) before immersion and after immersion in a Hanks' solution for (b) 6 h, (c) 24 h, (d) 3 d and (e) 7 d.

immersion in the Hanks' solution for 3 d.[18] The precipitates grew with time, and finally identified as hydroxyapatite by XRD after immersion for 14 d. In the present study, the precipitates were too small to be determined by XRD, but analyzed as a Ca-P-O compound by energy-dispersive X-ray spectroscopy (EDS). The Ca/P molar ratio were rather scattered in the range between 1.1 and 1.4 due to too small sizes. These precipitates may be a kind of embryo or perform of apatite.

Figure 9 shows the surface morphology of HAp film prepared on CP-Ti substrate at $P_L = 50$ W and $P_{tot} = 0.6$ kPa before and after immersion in a Hanks' solution. No changes were observed until 24 h of immersion (Fig. 9(b), (c)). Spherical particles were preferentially precipitated along the grain boundaries of cone texture in the HAp film after 3 d (Fig. 9(d)). Sugino *et al.* studied the hydroxyapatite regeneration on two pieces of pre-oxidized V-shaped Ti plates changing the distance between the Ti plates.[24–26] They demonstrated the regeneration of hydroxyapatite on both facing Ti surfaces after immersing in a simulated body fluid. The regeneration of hydroxyapatite strongly depended on the distance, and was significant at a narrow spacing less than 0.6 mm. In the present study, the regeneration at a narrow space such as the boundaries of cone texture was evident as shown in Fig. 9(d). After 7 d, needle-like precipitates wholly covered the surface of HAp films (Fig. 9(e)). For both of the MOCVD and LCVD HAp films, the precipitates were formed preferentially at the grain boundaries. However, the regenerated precipitates wholly covered the MOCVD HAp films within 6 h, which was much faster than that of LCVD HAp films. MOCVD HAp films consisted of granular grains in sub-micron size whereas LCVD HAp films composed of large grains 1 to 3 μm in size. The LCVD HAp grains had a flat surface probably due to high crystallinity. In our previous studies on the MOCVD $CaTiO_3$ films, the regeneration rate of hydroxyapatite on a complicated surface was much faster than that on a flat surface. The flat surface of large grains with high crystallinity of LCVD HAp films might have resulted in a slow regeneration rate.

4. Conclusion

Ca-P-O films were prepared on a CP-Ti substrate by LCVD. β-TCP films in a single phase were obtained at $T_{dep} > 900$ K, $R_{Ca/P} < 0.4$ and $P_L = 50$ W, while HAp films in a single phase were obtained at $P_L = 50$ W, $T_{dep} > 900$ K, $R_{Ca/P} > 1.0$ and $T_{dep} < 900$ K, $R_{Ca/P} > 0.45$. The surface morphology of β-TCP films showed an elongated and angular roof-shaped texture with a (220) orientation. The surface morphology of HAp films had a granular texture with a (300) orientation. Spherical apatite crystals were regenerated at hollow places on β-TCP and HAp films after 3 d. Needle-like apatite crystals covered the whole surface of HAp films after 7 d.

Acknowledgements

This study was partially supported by the Japan Society for the Promotion of Science (JSPS), Grant-in-Aids for Scientific Research (B), 18360310, Grant-in-Aids for JSPS fellow, global COE "Materials Integration", Tohoku University, Asian CORE program and Research and Education Funding for Inter-University Research Project, MEXT, JAPAN.

REFERENCES

1) M. Papakyriacou, H. Mayer, C. Pypen, H. Plenk Jr. and S. Stanz-Tschegg: Int. J. Fatigue **22** (2000) 873–886.
2) A. Yamamoto, R. Honma and M. Sumita: J. Biomed. Mater. Res. **39** (1998) 331–340.
3) P. I. Branemark, U. Breine, R. Adell, B. O. Hansson, J. Lindstrom and A. Ohlsson: Scand. J. Plast. Reconstr. Surg. **3** (1969) 81–100.
4) P. I. Branemark: J. Prosthet. Dent. **50** (1983) 399–410.
5) D.-M. Liu, T. Troczynski and W. J. Tseng: Biomaterials **22** (2001) 1721.
6) W. Wheng: J. Am. Ceram. Soc. **82** (1999) 27.
7) H. Ji, C. B. Ponton and P. M. Marquis: J. Mater. Sci.: Mater. Med. **3** (1992) 283.
8) I. Baltag, K. Watanabe, H. Kusakari, N. Taguchi, O. Miyakawa, M. Kobayashi and N. Ito: J. Biomed. Mater. Res. **53** (2000) 76.
9) T. Narushima, K. Ueda, T. Goto, H. Masumoto, T. Katsube, H. Kawamura, C. Ouchi and Y. Iguchi: Mater. Trans. **46** (2005) 2246–2252.
10) K. Yamashita, T. Arashi, K. Kitagaki, S. Yamada and T. Umegaki: J. Am. Ceram. Soc. **77** (1994) 2401.
11) H. M. Kim, F. Miyaji, T. Kokubo and T. Nakamura: J. Biomed. Mater. Res. A **32** (1996) 409–417.
12) M. Uchida, H. M. Kim, T. Kokubo, S. Fujibayashi and T. Nakamura: J. Biomed. Mater. Res. B **63** (1996) 522–530.
13) R. Tu and T. Goto: Mater. Sci. Forum **475–479** (2005) 1219–1222.
14) T. Kimura and T. Goto: Mater. Trans. **44** (2003) 421–424.
15) M. Sato, R. Tu and T. Goto: Mater. Trans. **47** (2006) 1386–1390.
16) M. Sato, R. Tu and T. Goto: Mater. Trans. **48** (2007) 3149–3153.
17) M. Sato, R. Tu, T. Goto, K. Ueda and T. Narushima: Mater. Trans. **48** (2007) 1505–1510.
18) M. Sato, R. Tu, T. Goto, K. Ueda and T. Narushima: Mater. Trans. **49** (2008) 1848–1852.
19) M. Sato, R. Tu, T. Goto, K. Ueda and T. Narushima: J. Ceram. Soc. Jpn. **117** (2009) 461–465.
20) D. W. Lynch and W. R. Hunter: *Handbook of optical constants of solids*, (1985) 240–249.
21) F. Gervais: *Handbook of optical constants of solids*, (1985) 761–775.
22) P. M. deWolff: Technisch Physische Dienst, Delft, The Netherlands, ICDD Grant-in-Aid, PDF #09-0169.
23) J. Dong, T. Uemura, Y. Shirasaki and T. Tateishi: Biomaterials **23** (2002) 4493–4502.
24) A. Sugino, K. Uetsuki, K. Tsuru, S. Hayakawa, A. Osaka and C. Ohtsuki: Mater. Trans. **49** (2008) 428–434.
25) X. X. Wang, S. Hayakawa, K. Tsuru and A. Osaka: J. Biomed. Mater. Res. **54** (2001) 172–178.
26) X. X. Wang, W. Yan, S. Hayakawa, K. Tsuru and A. Osaka: Biomaterials **24** (2003) 4631–4637.